Measurement of Magnetic Properties at High Temperature and Application to Magneto-Thermal Coupled Analysis of Induction Heater

Norio Takahashi
Department of Electrical and Electronic Engineering,
The Graduate School of Natural
Science and Technology, Okayama University
3-1-1 Tsushima-naka, Kita-ku, Okayama 700-8530, Japan

Abstract :
Abstract: The magnetic properties of magnetic materials are considerably changed near the Curie temperature. The consideration of the temperature dependence of the B-H curves and iron loss curves is necessary for the precise analysis. In this paper, the measuring method of magnetic properties at high temperature using ring specimens is examined, and a technique to improve the accuracy is investigated. The eddy current and temperature distribution of an induction heater are analyzed considering temperature dependence of magnetic characteristics which is measured by us.
It is shown that the calculated values of temperature are in good agreement with measured values.

Keywords:
Magnetic Properties, High Temperature, Induction Heating, Coupled Analysis

1. Preface

The BH characteristics of magnetic materials such as billet used to produce the while axis of automobiles varies with temperature. Especially near the Curie temperature where the permeability dramatically decreases. The temperature inside billet varies with time. Therefore, a coupled analysis of the eddy currents and temperature needs to be performed using the material constants such as permeability, resistivity, and specific heat for the temperature in each area for each time step to utilize a coupled analysis that takes into account the variations of the permeability distribution in billet versus time. [(1)]Material properties for high temperatures need to be used when analyzing the characteristics of electromagnetic devices used in vehicles because vehicles can reach temperatures of more than 150 degrees Celsius. [(2)] There are very few examples measuring material properties at temperatures near the Curie point. Therefore, this research considers methods to measure material properties at Curie temperatures using ring specimens and investigates the accuracy of the results. Furthermore, problems in measuring this phenomena is examined, such as methods for raising temperatures during measurement.

In this paper, the magnetic characteristics of various materials are measured using a measurement system for measuring magnetic characteristics at high temperatures, and then describes the differences of the magnetic characteristics that occur in the materials at high temperatures. In addition, a coupled thermal and magnetic field analysis of a billet heater, which is used as the induction heating devices, is performed and the couple analysis procedure as well as the eddy current loss and temperature versus time for each part inside the billet are clarified. The validity of the simulation results are examined by comparing actual measured values. The temperature dependency of the BH curve is considered by comparing results that account for the temperature dependency of BH curves and those that do not.

2. Examining Methods for Measuring Magnetic Characteristics of Magnetic Materials at High Temperatures

<2.1> Creating a Test Piece to Measure at High Temperatures

The insulation of the electric wire and test piece need to be innovated so that they are not ruined at temperatures such as the Curie point of steel. Therefore, a ring specimen was created using a guard vessel and heat resistant insulation tap. The guard vessel indicated in Fig. 1 is a ceramic material that can withstand temperatures of up to 1000 degrees Celsius with 4 ring specimens (inner diameter: 70 mm; outer diameter: 100 mm) of non-oriented electromagnetic steel sheet inside. The ring specimens are extracted by using a wire cut that accounts for the effects of stress. The test piece that was created is indicated in Fig. 2. The white tap covering the exterior is thermal resistant tape providing insulation up to 1000 degrees Celsius. The exciting coil is wrapped with insulation every turn to withstand the heat. The tap is also warped between each test piece. A cross-section of the test piece that was created is

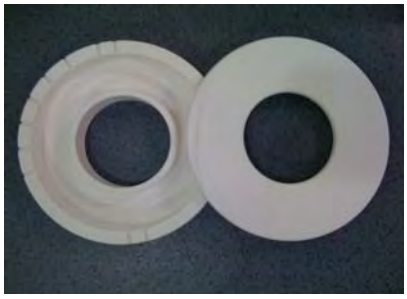

(a) External appearance

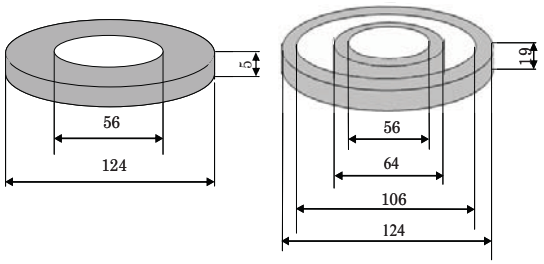

(b) Container diameter

Fig 1. Conservation container

indicated in Fig. 3.

The cross-sectional area of the B coil used to examine the magnetic flux density of the test piece because the thermal insulation tape is used to reinforce the test piece and insulation of wire for this research even though the B coil is usually wound directly to the test piece.

The insulation tape is warp around the outside of the protection container to make compensating for the air gap easier by confirming the cross-section of the B coil. Furthermore, the B coil has 20 turns using wire that has a diameter of 1 mm. The exciting coil producing the magnetic field is wound using 70 turns wrapping thermal insulation tape after each turn by manually operating an automatic toroidal coil winding machine model 100 (TAGA CO. LTD) using wire that has a diameter of 1.4 mm.

Fig. 2 Test piece to measure at high temperatures

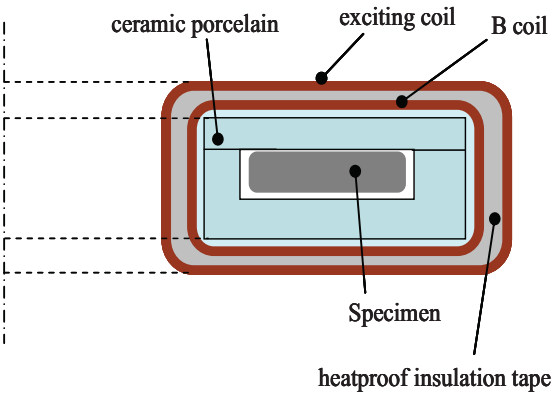

Fig. 3 Cross-section of test piece

<2.2> Measuring Method

A block diagram of the measuring system that was used is indicated in Fig. 4. The exciting frequency is 50 Hz. The magnetic flux density B is obtained by importing data calculated by amplifying the induced voltage detected in the B coil using a single amplifier and converting with an A/D converter to a computer, and then integrating using the discrete Fourier transform. The magnetic field intensity is also obtained using the excitation current method from the current flowing in the shunt resistance. The test piece is placed in the furnace indicated in Fig. 5 and the coil and thermocouple are connected by innovating the furnace door.

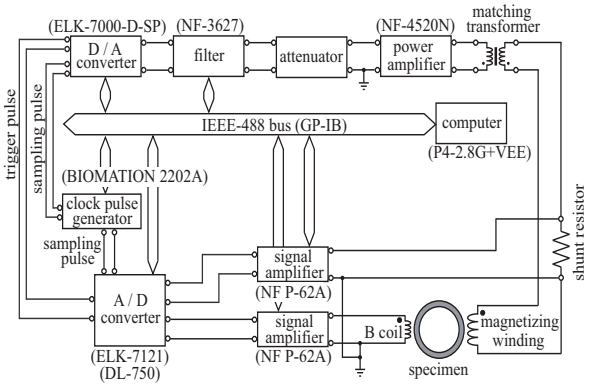

Fig. 4. Measuring system

<2.3> Compensating for the Air Gap

The B coil detecting the magnetic flux density in the test piece has an air gap between the B coil and the test piece because the thermal insulation tape is wrapped around the guard vessel for the reasons described in <2.1>. Therefore, the magnetic flux flowing the air gap in the B coil is included in the magnetic flux Bmea detected by the B coil. Evan though the magnetic flux can be obtained using the magnetic flux passing through the test piece, the magnetic flux density needs to compensate for the air gap because the induced voltage caused by the flux passing through the air gap is also output to the B coil. Therefore, the magnetic flux Φspe passing through the test piece is obtained by subtracting the magnetic

Fig. 5. Furnace increasing temperature

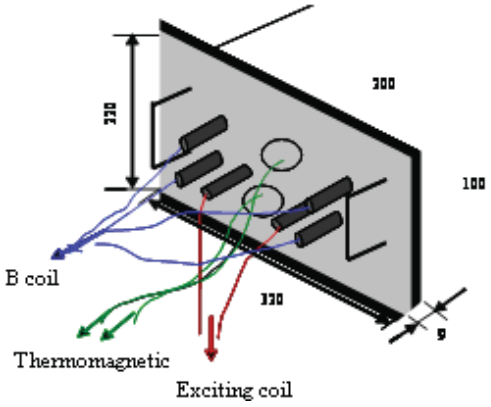

Fig. 6 Furnace door

flux passing through the air gap from teh flux linkage in the B coil using equation (1), and then the magnetic flux Bspe in the test piece is obtained using equation (2). [4][6]

$$\Phi_{spe} = B_{mea} S_{spe} - \mu_0 H_{mea} S_{air} \quad (1)$$

$$B_{spe} = \frac{\Phi_{spe}}{S_{spe}} \quad (2)$$

Sspec is the area of the test piece's cross-section, Sair is the area of the air gap's cross-section, and Hmea is the magnetic field intensity that is measured.

<2.4> Accuracy of Measurements for Curie Temperatures

This section describes the validity of compensating for the air gap described in <2.3> is examined. The results of the relative permeability measured above the Curie temperature are indicated in Fig. 7. The relative permeability obtained by compensating for the air gap measures approx. 1.03 with a 3% error.

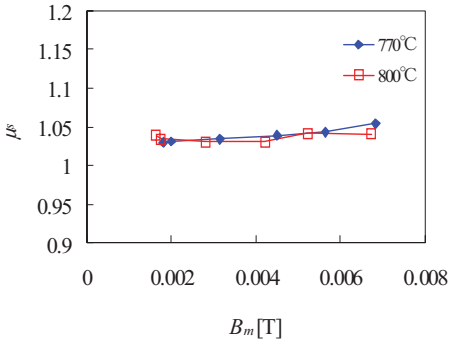

Fig. 7. Relative permeability above Curie temperature (35A250/50 Hz)

First, the difference between the average length of magnetic paths that were measured and the actual length of the magnetic paths is examined to investigate the cause of the error. [4]The magnetic field intensity, H, above the Curie temperature without magnetic properties is indicated in Fig. 8. The average length of the magnetic pathway, Lmean, is 0.2669 m which can be calculated with equation (3) using r_1 as the interior radius and r_2 as the exterior radius.

$$Lmean = \pi(r_1 + r_2) \quad (3)$$

If the ampere turns of the coil for the magnetic flux intensity, H, at the point of radius r in the test piece is NI, the actual width of the magnetic pathways is 0.2640 m which can be calculated using equations (4) and (5).

$$Leff = \frac{1}{r_2 - r_1} \int_{r_1}^{r_2} Hdr \tag{4}$$

$$H = NI / 2\pi r \tag{5}$$

This indicates a error of 1.1% between Lmean and Leff above the Curie point.

The steel expands at a constant expansion coefficient as the temperature rises. Therefore, the cross-sectional area of the test piece varies as it expands with rising temperatures. The cross-sectional area of the test piece is $21.41 \times 10^{-6}m^2$obtained using the expansion coefficient of steel (0.00968) at 800 degrees Celsius, which has a 2% difference from the original cross-sectional area for the test piece of $21.0 \times 10^{-6}m^2$. A 3% error can be expected based on the two evaluation results above. Further examination of the measurement accuracy between room temperature and the Curie point is necessary in the future.

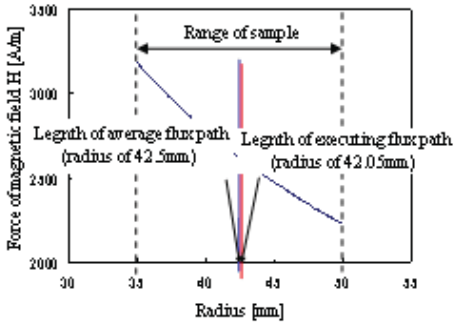

Fig. 8. Width of magnetic pathways

<2.5> Examining the Raising Temperatures

Measurements at each of the various temperatures are not feasible because it would take approximately a week of continuous measurements. Therefore, the temperatures could be measured by raising the temperature after measuring up to a certain point and the reducing the temperature. The measurements were performed by raising the temperature to T_1 degrees Celsius, and then lowering the temperature. The next day the measurements were performed by raising the temperature to T_2 degrees Celsius, and then raised gain to T_2 degrees Celsius ($T_2 > T_1$) to see if there is a difference in the results. (5)

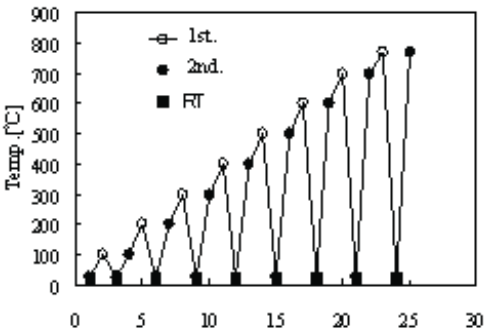

Fig. 9. Temperature pattern

The measurements were taken for the temperature pattern indicated in Fig. 9 for a frequency of 50 Hz up to the Curie temperature of (770 degrees Celsius). More specifically, the temperature was first (1st time) raised to 100 degrees Celsius (T_{100}, ○ mark), and then the temperature was lowered to room temperature before raising the temperature to 100 degrees Celsius (T_{100}*, ● mark) again (2nd time). The measurements were then taken by raising the temperature up to 200 degrees Celsius (T_{200}) and the results were reviewed to see if there was a difference in T_{100} and T_{100}*.

The relative permeability, μ_s, measured the 1st time (T_{100}, T_{200}…) is indicated in Fig. 10(a) and the difference between the results, η, measured the 1st and 2nd time are indicated in Fig. 10 (b) (n=100,200 …).

$$\eta = \left\{ \left(\frac{\text{Measured result for } T_n^*}{\text{Measured result for } T_n} \right) - 1 \right\} \times 100 \tag{6}$$

η is within 5% for the relative permeability. The results measured the 2nd time are larger. The relative permeability at the Curie point indicated in Fig. 11 are accurate considering the measurements the 1st and

2nd time are almost μ_s=1.

The difference in the measured values comparing the 2nd time to the 1st time at the next lower temperature has an error within 10%. This method can be applied to measure the raising temperatures because the error will not drastically change the characteristics when evaluating the temperature characteristics of magnetic materials.

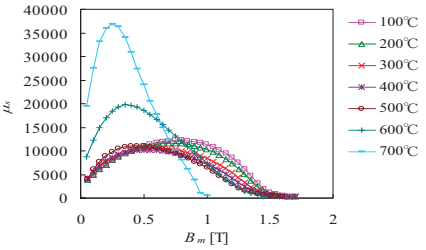

(a) 1st time (T100, T200…) results

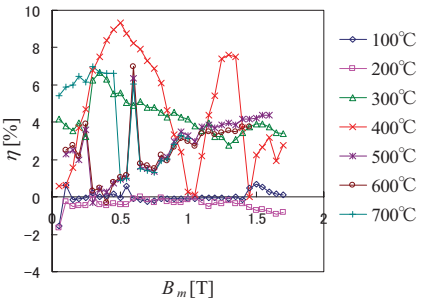

(b) Comparing 1st and 2nd time

Fig. 10. Relative permeability

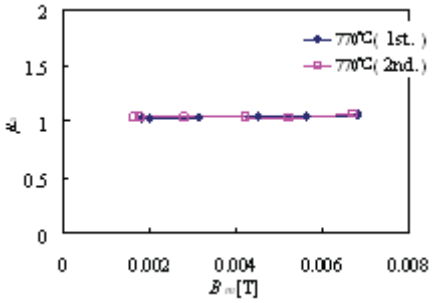

Fig. 11 Relative permeability at 700 ℃

3. Magnetic Properties of Magnetic Materials at High Temperatures

<3.1> Magnetic Properties of Various Magnetic Materials

The BH curves of cooled rolled steel sheet SPCC (thickness: 1 mm), rolled steel for general structures SS400 (thickness: 0.6 mm), non-oriented electromagnetic steel 35A250 (thickness: 0.35 mm), and 6.5% Si steel sheet are indicated in Fig. 12. The relative permeability, μ_s, that was measured is indicated in Fig. 13. [7),(20)] The temperature dependency of the relative permeability, μ_s, is indicated in Fig. 14. The way the relative permeability varies as the temperature raises differs depending on the material as indicated in Fig. 13. The magnetic flux gradually decreases as the relative permeability reaches a maximum when the temperature rises for 35A250 and 6.5% Si and the magnetic flux has a maximum of approx. 0.25 T at 700 degrees Celsius. On the other hand, the magnetic flux at the maximum relative permeability up to 600 degrees Celsius is roughly 0.8 T without varying and remains at approx. 0.6 T even at 700 degrees Celsius. The temperature and μ_s increases at 0.25 T and a line similar to the Hopkinson effect, as indicated in Fig. 14. The temperature and μ_s increase at 0.8 T In materials that has a very low μ_s such as SPCC, but the temperature and μ_s vary little as the magnetic flux density increases in material with a high μ_s such as 35A250. Furthermore, the temperature and μ_s decrease for both materials at 1.5 T.

The iron loss that is measured is indicated in Fig. 15 and the iron loss versus temperature is indicated in Fig. 16. The iron loss decreases with the temperature regardless of the size of the magnetic flux density, but the ratio iron loss is reduced by temperature is larger for SPCC. The separated results of the iron loss at 50 Hz are indicated in Fig. 17. The hysteresis loss decreases with the temperature raises. Therefore, the hysteresis loss is a phenomenon that increases at lower temperatures [8)(9)]. The eddy current loss also decreases with the temperature, but the conductivity decreases at high temperatures, as indicated in Fig. 18.

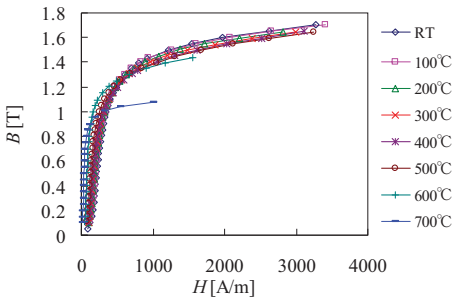

(a) SPCC

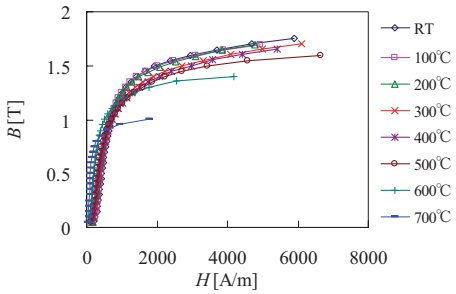

(b) SS400

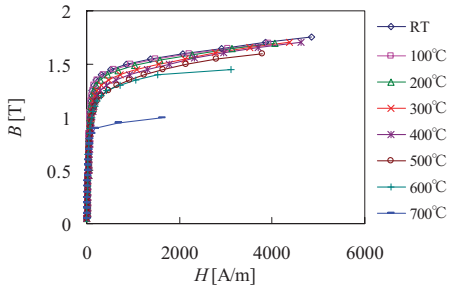

(c) 35A250

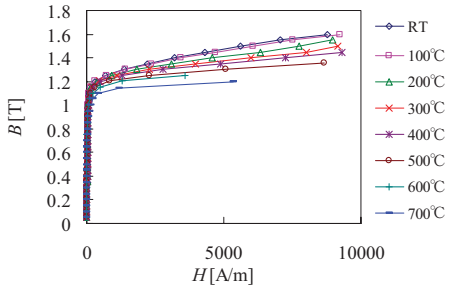

(d) 6.5% Si steel

Fig. 12 Temperature characteristics of BH curve

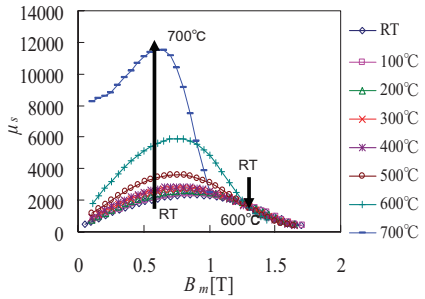

(a) SPCC

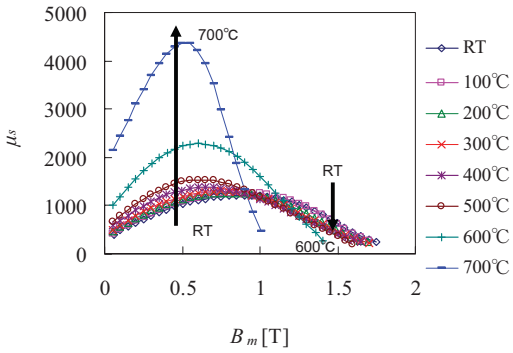

(b) SS400

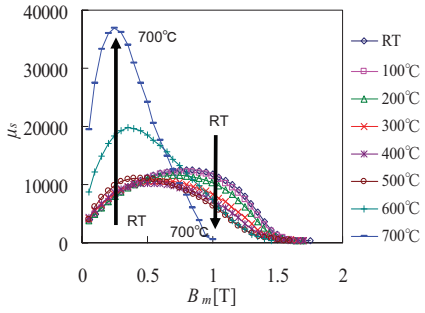

(c) 35A250

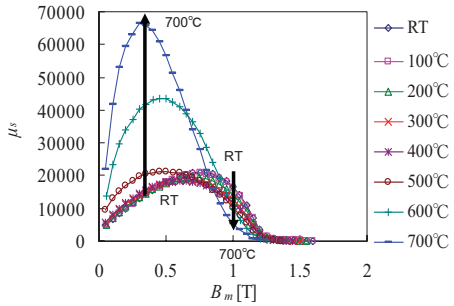

(d) 6.5% Si steel

Fig. 13. Temperature characteristics of permeability

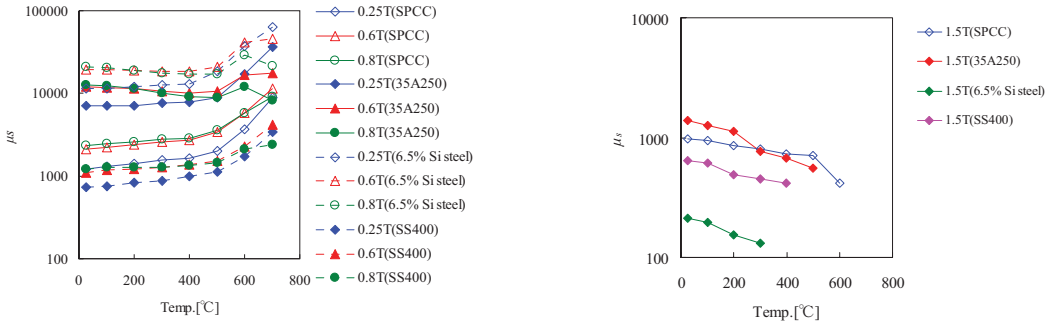

(a) $Bm > 0.8$T (b) Bm=1.5T

Fig. 14. Variations of permeability by temperature

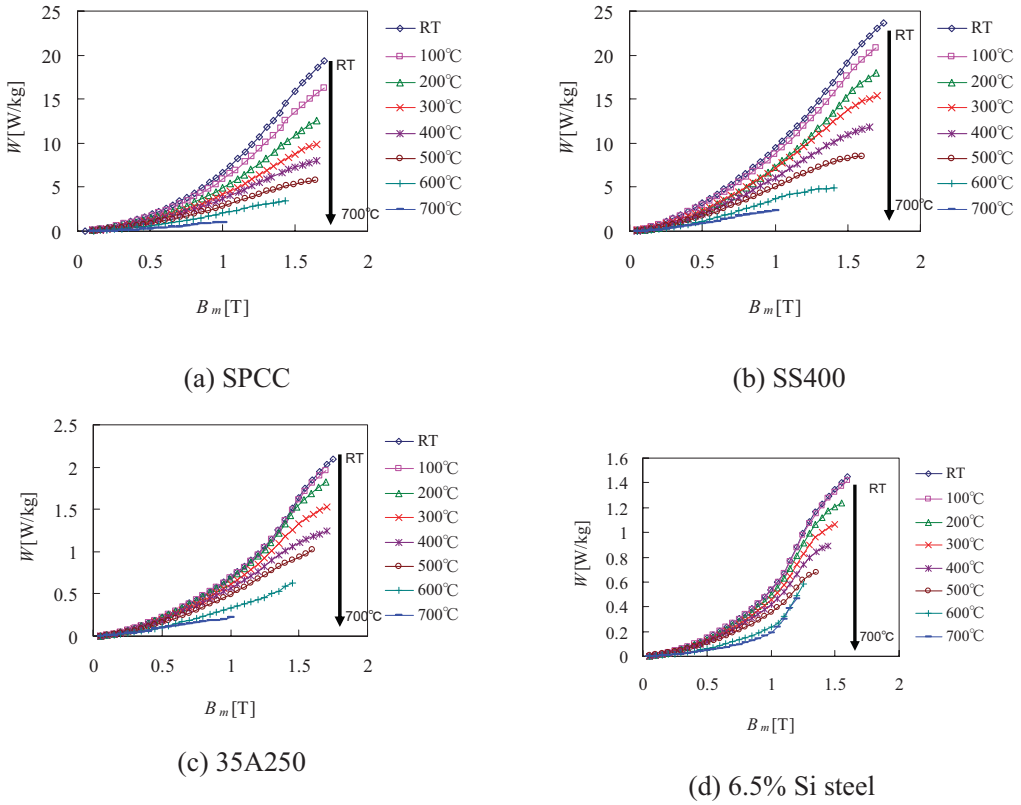

(a) SPCC (b) SS400

(c) 35A250 (d) 6.5% Si steel

Fig. 15. Temperature characteristics of iron loss

The SPCC is thick in this testing and has a ratio of eddy currents in all of the steel sheets that is larger than the 6.5% Si. The SPCC also has conductivity that varies largely by temperature as indicated in Fig. 18 (approx. 2 times 6.5% Si). Therefore, the iron loss decreases largely with the temperature for the SPCC.

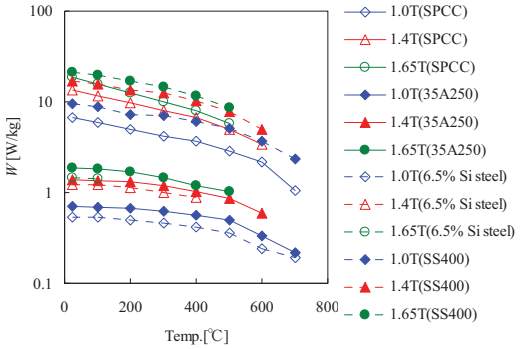

Fig. 16 Variation of iron loss by temperature

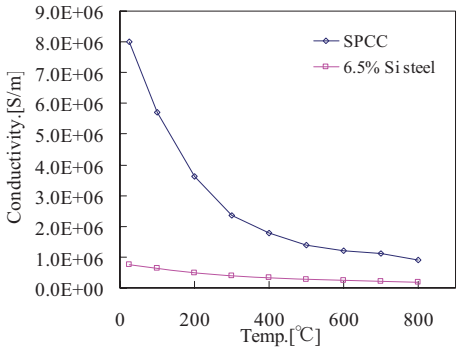

Fig. 18 Temperature characteristics of conductivity

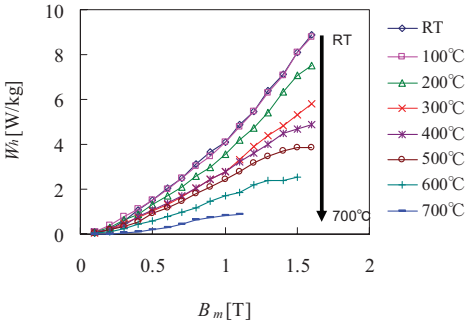

(i) SPCC

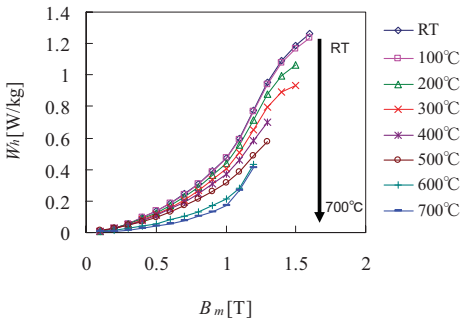

(ii) 6.5% Si steel

(a) Hysteresis loss

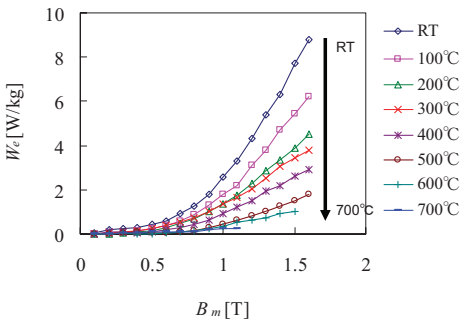

(i) SPCC

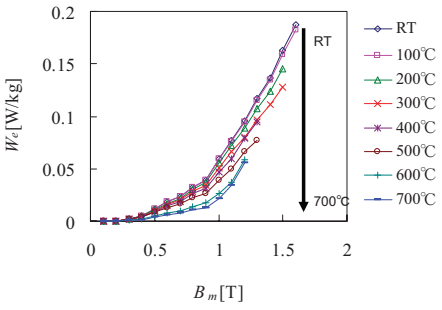

(ii) 6.5% Si steel

(b) Eddy current loss

Fig. 17 Temperature characteristics of hysteresis loss and eddy current loss

<3.2> Effects of Magnetic Characteristics at Room Temperature

The magnetic characteristics are measured by raising the temperature by 100 degree Celsius until the Curie point is reached, and then measuring again after the test piece has cooled to room temperature naturally to investigate the effects on magnetic characteristics at room temperature.

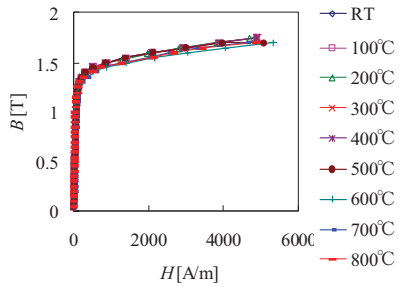

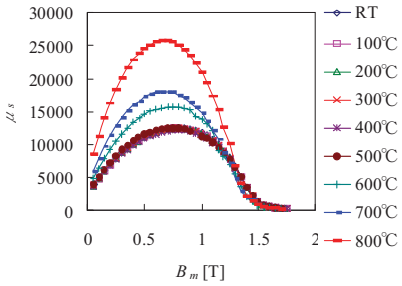

(b) μs-*B*m curve

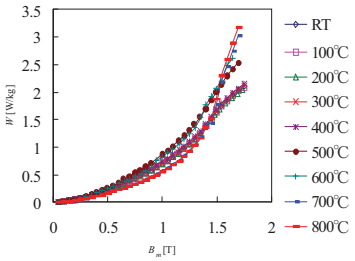

(c) *W-Bm* curve

Fig. 19. Variations of magnetic properties at the tested temperatures from room temperature (35A250, 50Hz)

The magnetic properties that are measured at room temperature (RT) for 35A250 in Fig. 9 are indicated in Fig. 19. The tested temperatures are indicated in the legend on the right side of the diagram. The relative permeability and iron loss versus temperature are indicated in Fig. 20. The relative permeability increase to 1.0 T when the temperature is above 500 degrees Celsius, but then moderately decreases above 1.2 T. Furthermore, the iron loss does not vary for each magnetic flux density up to 400 degrees Celsius, but, as the temperature reaches 500 degrees Celsius, the line increases 0.4 T where there had been no variations from 0.2T. Therefore, the degree the relative permeability increases is larger for higher magnetic flux densities. The line decreases after 600 degrees Celsius excluding 1.6 T and there is very little variation between 700 degrees Celsius and 800 degrees Celsius. This is similar to the variations of μ_s and W caused by the temperature in Fig. 15 and Fig.16. For this reason, the relative permeability is high when the magnetic flux density is low if magnetic materials are subjected to high temperatures indicating the iron loss decreases or phenomena similar to an anneal effect is happening. Therefore, machines driven in regions with a relatively low magnetic flux density improve their magnetic characteristics after being exposed to high temperatures.
Furthermore, 35A250 maintains its magnetic characteristics up to temperatures of 400 degrees Celsius based on the relative permeability and iron loss results above.

4. Couple Thermal and Magnetic Field Analysis of an Induction Heating Device

<4.1> Analysis Model and Analysis Conditions

The billet heater used for this analysis is indicated in Fig. 21. The billet material is S45C and the structure has the heat insulation wrapped around the fire-resistant material. The Curie temperature of the billet material is 760 degrees Celsius.

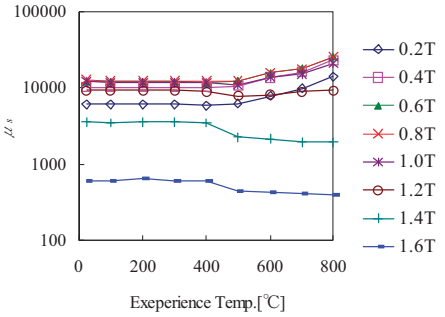

(a) μs-Experience Temp. curves

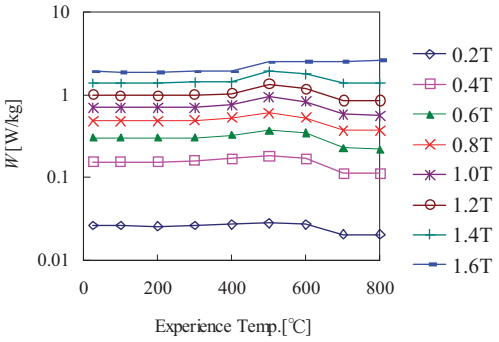

(b) W-Experience Temp. curves

Fig. 20 Effects on relative permeability and iron loss for temperatures rising from room temperature (35A250, 50 Hz)

The magnetic field analysis used the 3D finite element method with edge elements [10] and the A-method and the thermal analysis uses the 3D nodal finite element analysis. The coil is divided in the actual machine as indicated in Fig. 21, but it is considered uniform in the Z direction as indicated in Fig. 22. For example, the heat sources of the billet is calculated by performing a finite element analysis of the cross-section (Fig. 23) indicated in *a*-*a*' of Fig. 22, and then the distribution is calculated when the billet is displaced in the Z direction. However, excitation is performed for the actual coil arrangement so that the moment the *a*-*a*' cross-section is between the coil in Fig. 21 the current does not flow in the coil in Fig. 23. Furthermore, the initial temperature of each material is 25 degrees Celsius and the boundary of he analysis regions are specified as heat insulation boundaries. [11][12]

<4.2> Coupled Thermal and Electromagnetic Field Analysis

The temperature field was analyzed based on the following governing equations for 3D transient heat transfer. [13]

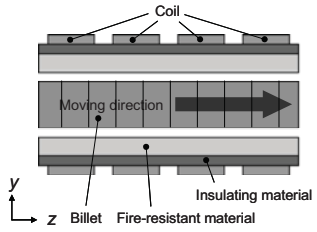

(a) *z*-*y* plane

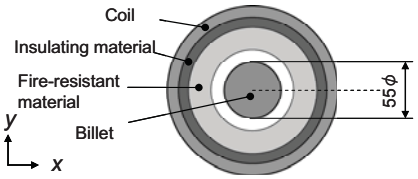

(b) *x*-*y* plane

Fig. 21 Billet heater

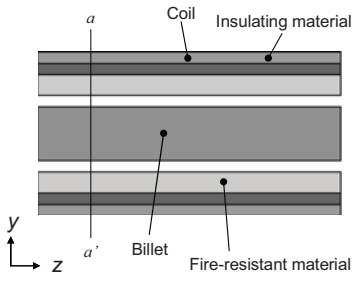

Fig. 22. Uniform model in Z direction

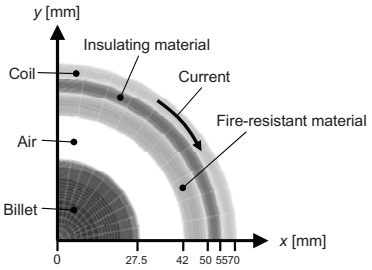

Fig. 23. Analysis model (1/4 model)

$$\frac{\partial}{\partial x}\left(\lambda_{xx}\frac{\partial T}{\partial x}\right)+\frac{\partial}{\partial y}\left(\lambda_{yy}\frac{\partial T}{\partial y}\right)+\frac{\partial}{\partial z}\left(\lambda_{zz}\frac{\partial T}{\partial z}\right)+Q=\rho c\frac{\partial T}{\partial t} \tag{7}$$

The T is the temperature of the heated body, λ is the heat transfer, Q is the internal heat sources, ρ is the density, c is the specific heat, and t is the time.

The boundary condition for the heat transfer if the heat flux is q, and the normal vector in the outer direction of the boundary is $\boldsymbol{n}$ can be found with the following equation using the Fourier's law.

$$q=-[\lambda]\frac{\partial T}{\partial \boldsymbol{n}}=-[\lambda](\boldsymbol{n}\cdot\nabla T)=-\begin{bmatrix}\lambda_{xx}&0&0\\0&\lambda_{yy}&0\\0&0&\lambda_{zz}\end{bmatrix}\begin{bmatrix}\frac{\partial T}{\partial x}n_x\\\frac{\partial T}{\partial x}n_y\\\frac{\partial T}{\partial x}n_z\end{bmatrix} \tag{8}$$

The governing equation for the heat conductivity problem was discretized using the 3D nodal elements. The following equation is obtained by discretizing the governing equations using $\{N\}$ as the interpolation equation.

$$\begin{aligned}&\iint_S q\{N\}^{\mathrm{T}}\,dS\\&+\iiint_V\left\{\frac{\partial\{N\}}{\partial x}\left(\lambda_{xx}\frac{\partial\{N\}^{\mathrm{T}}}{\partial x}\right)+\frac{\partial\{N\}}{\partial y}\left(\lambda_{yy}\frac{\partial\{N\}^{\mathrm{T}}}{\partial y}\right)\right.\\&\left.+\frac{\partial\{N\}}{\partial z}\left(\lambda_{zz}\frac{\partial\{N\}^{\mathrm{T}}}{\partial z}\right)\right\}dV\{T\}_e-\iiint_V Q\{N\}dV\\&+\iiint_V \rho c\{N\}\{N\}^{\mathrm{T}}\,dV\frac{\partial\{T\}_e}{\partial t}=0\end{aligned} \tag{9}$$

The temperature field analysis was performed by adding the boundary conditions to the above equation.

The amount of heat that is radiated, q, is applied to the following equation when heat is radiated to the surrounding environment along the fixed boundary. (13)(14)

$$\begin{aligned}&q=h(T-T_{\mathrm{out}})\\&h=\varepsilon\sigma F(T+T_{\mathrm{out}})(T^2+T_{\mathrm{out}}^2)\end{aligned} \tag{10}$$

ε is the thermal emissivity, σ is the Stefan-Blotzman constant, F is the configuration factor, T_{out} is the surrounding environment temperature, and h is the coefficient for radiated heat. The analysis is performed by substituting the value in the previous step for the unknown T.

The following equation is obtained by substituting the boundary integral component of equations (9) and (10) (first component on left).

$$\begin{aligned}\iint_S q\{N\}^{\mathrm{T}}\,dS&=\iint_S h(T-T_{\mathrm{out}})\{N\}dS\\&=\iint_S h\{N\}\{N\}^{\mathrm{T}}\,dS\{T\}_e-\iint_S hT_{\mathrm{out}}\{N\}dS\end{aligned} \tag{11}$$

The discretization equation of the heat transfer problem including the boundary condition is as follows:

$$[K]\{T\}+\{C\}\left\{\frac{\partial T}{\partial t}\right\}=\{F\} \tag{12}$$

$[K]$ is the heat conductivity matrix, $[C]$ is the thermal capacity matrix, $\{F\}$ is the thermal flow vector indicated in the following equation:

$$[K]=\iiint_V \left\{ \frac{\partial\{N\}}{\partial x}\left(\lambda_{xx}\frac{\partial\{N\}^{\mathrm{T}}}{\partial x}\right)+\frac{\partial\{N\}}{\partial y}\left(\lambda_{yy}\frac{\partial\{N\}^{\mathrm{T}}}{\partial y}\right) + \frac{\partial\{N\}}{\partial z}\left(\lambda_{zz}\frac{\partial\{N\}^{\mathrm{T}}}{\partial z}\right)\right\}dV+\iint_S h\{N\}\{N\}^{\mathrm{T}}dS \tag{13}$$

$$[C]=\iiint_V \rho c\{N\}\{N\}^{\mathrm{T}}dV \tag{14}$$

$$\{F\}=\iiint_V Q\{N\}^{\mathrm{T}}dV+\iint_S hT_{\mathrm{out}}\{N\}^{\mathrm{T}}dS \tag{15}$$

A coupled electromagnetic and thermal analysis is run using the following procedure to account for the conductivity, permeability, specific heat, and temperature variations of the thermal conductivity for the billet. First, a magnetic field analysis using the 3D finite element method was performed by applying a material constant with an initial temperature (25 degrees Celsius) to obtain the eddy current loss of the billet heater by solving the following basic equation.

$$\mathrm{rot}\left(\nu\,\mathrm{rot}\boldsymbol{A}\right)=J_0-\sigma\left(\frac{\partial\boldsymbol{A}}{\partial t}+\mathrm{grad}\phi\right) \tag{16}$$

Next, a thermal analysis was performed by using the eddy current loss obtained in the magnetic field analysis as the heat sources to obtain the temperature distribution of the billet heater. Furthermore, the temperature distribution is obtained by obtaining the eddy current loss for the material constant at the raising temperatures. The temperature distribution for each time was obtained by repeating these two analyses. The time interval that was used is 1 second.

<4.3> Temperature Variations of Material Properties

The properties for the air gap, fire resistant material, and thermal insulation are indicated in Table 1. The thermal properties of the billet are indicated in Fig. 25 through Fig. 26. The linear interpolated values of data are used when running an analysis. The analysis was performed without taking into account the material properties of the fire resistant material, thermal insulation, and air because the objective is to examine the varying temperature distribution of the billet. '1' is used for the configuration factor in equation (10) for the billet and fire resistant material.

<4.4> Analysis Results and Evaluation

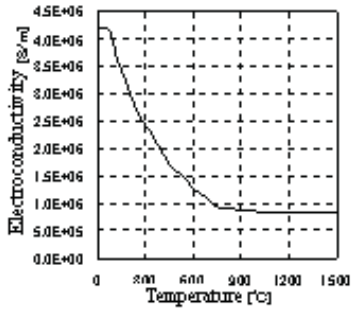

Fig. 24. Billet conductivity versus temperature

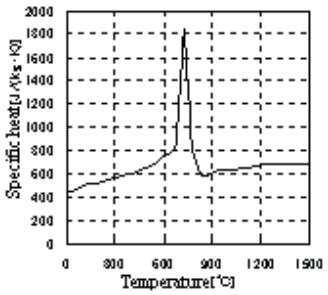

Fig. 25. Billet specific heat versus temperature

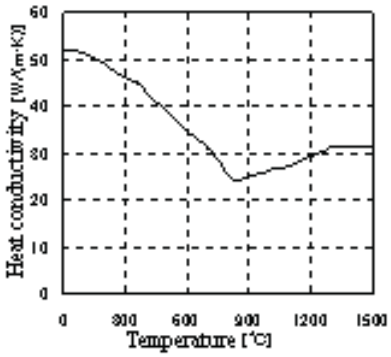

Fig. 26. Billet thermal conductivity

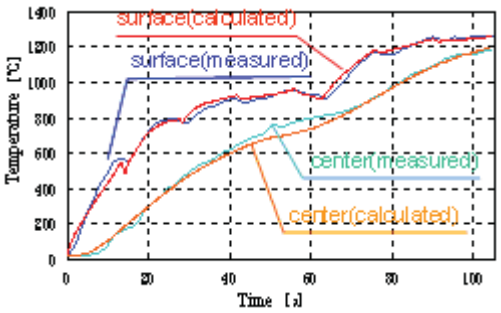

Fig. 27. Temperature versus time for the surface and center of the billet

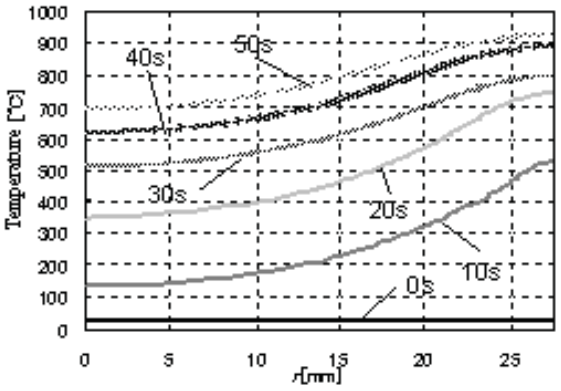

Fig. 28. Temperature distribution versus time of the Billet

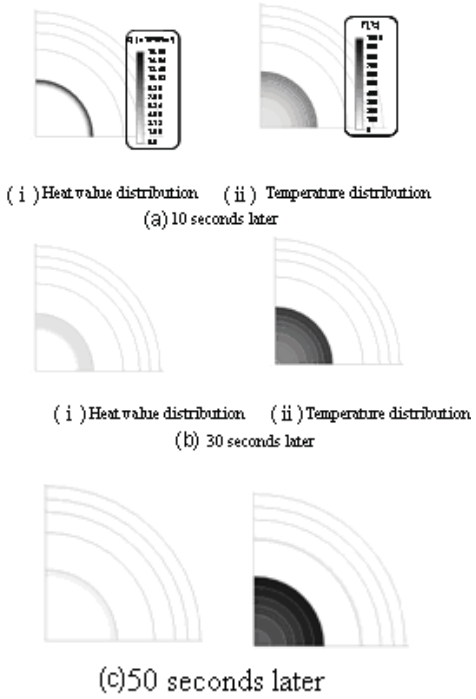

Fig. 29. Heat generation and temperature distribution of the billet

Table 1. Material properties at 25degrees Celsius

Material name	Specific heat [J/(kg·K)]	Heat conduction percentage λ [W/(m·K)]	Density ρ [kg/m³]	Emissivity
Billet (S45C)	444.1	51.9	7860	0.85
Fire-resistant material	1360	2.5	3160	0.7
Adiabatic material	1360	0.110	160	-

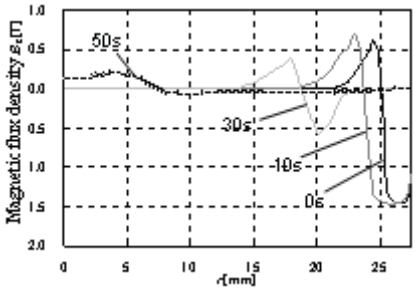

Fig. 30. Magnetic flux distribution versus time of the billet

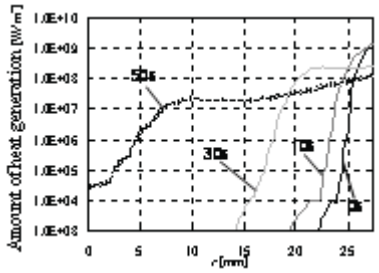

Fig. 31. Heat generation versus time of the billet

The temperature versus time for the center (r=0 mm) and the surface (r=27.5 mm) of the billet is indicated in Fig. 27, the temperature distribution versus time in Fig. 28, the heat generation distribution and temperature distribution in Fig. 29. The actual temperature measured using a thermal couple in Fig. indicated in Fig. 27.[16][17]

The actual results and analysis results for the raising temperature of the billet match well, as indicated in Fig. 17. The surface temperature is fluctuates suddenly every 20 seconds because the temperature of the billet reaches the Curie point and the specific heat suddenly rises.

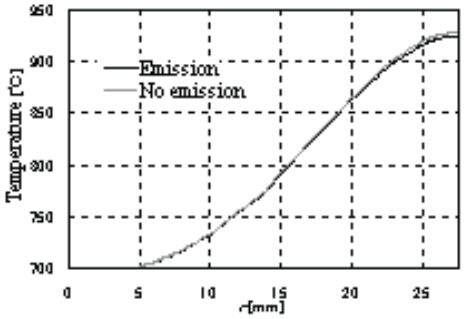

Fig. 32. Temperature distribution after heating stops (50 seconds) with and without radiation

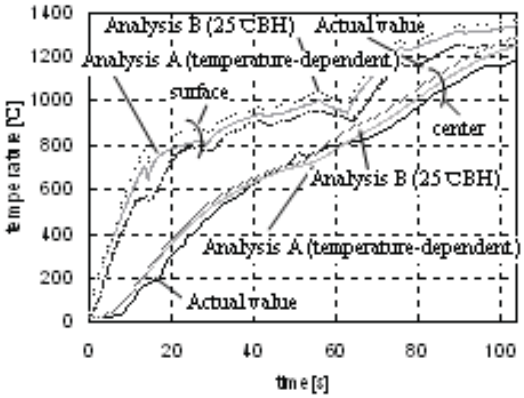

Fig. 33. Temperature versus time of the billet

The heat generation penetrates to the interior of the billet and its value decreases as the temperature rises, as indicated in Fig. 29. This is because the skin depth increases by the reduction in conductivity caused by raising temperatures, the magnetic flux decreases by the reduction in permeability, and the eddy currents that occur are smaller.

The magnetic flux density distribution versus time is indicated in Fig. 30 and the heat generation versus time in Fig. 31. The magnetic flux penetrates the billet and the magnetic flux density decreases because the permeability decreases by raising temperatures as time passes and the temperatures increase and in the billet. Therefore, the heat generated in the billet increases but the amount it increases is smaller.

The temperature distribution at the end of heating (50 seconds) with and without radiated heat is indicated in Fig. 32. The temperature on the surface of the billet decreases slightly when accounting for radiated heat, but the effect of the radiated heat is minimal because the temperature are still low at this point.

<4.5> Effects of the Temperature Dependence of the B-H Curve on the Analysis Results

This section compares the results with and without accounting for the temperature dependency of the B-H curve.

The temperature versus time for the center (r=0mm) and surface (r=27.5mm) of the billet when the temperature dependency of the B-H curve is taken into account (Analysis A) and when the relative permeability is 1 over the Curie point using a 25 degree Celsius B-H curve from room temperature to the Curie point (Analysis B) as well as the values measured with a thermocouple are indicated in Fig. 33. (18)(19)

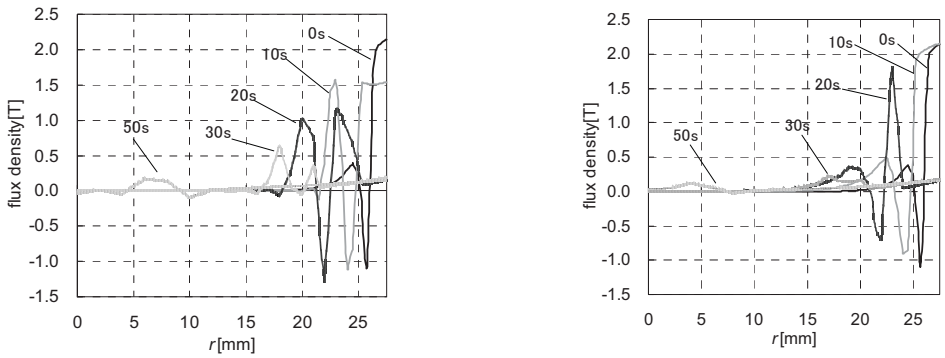

Fig. 34 Magnetic flux density distribution versus time for the billet

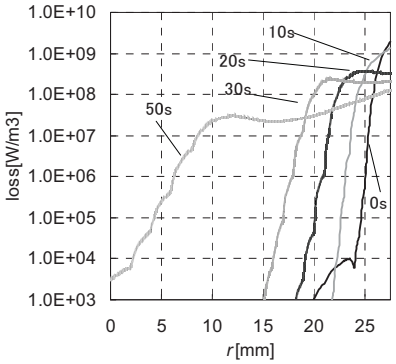

(a)Analysis A (with temperature dependency)

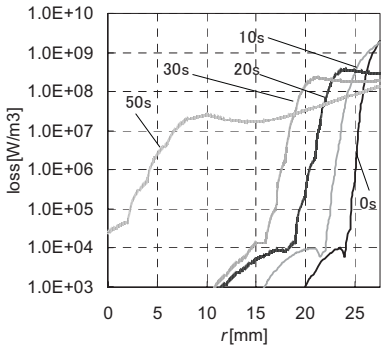

(b)Analysis B (with only 25℃B-H)

Fig. 35. Heat generation versus time of the billet

The temperatures in the analysis results are higher when comparing the analysis accounting for the temperature dependency of the B-H curve and actual values, but the rise in temperature is almost the same. The reason for the differing results could be the analyzing the z-direction uniformly. Furthermore, the temperatures are even higher for in Analysis B than Analysis A. The reason the results differ could be the following. The magnetic flux density is smaller on the surface because the permeability decreases as the temperature rises in Analysis A as indicated in Fig. 34. The magnetic flux density remains large on the surface of the billet for Analysis B up to the curie point where the permeability is 1 because the permeability is large as the temperatures rise. The temperature increases and continues to diverge because the heat generation is large in Analysis B especially around 10 seconds as indicated in Fig. 35. The results for Analysis B around the Curie point (15 seconds) in Fig. 31 is approx. 80 degrees Celsius (10%) higher on the surface than Analysis A and approx. 35 degrees Celsius (3%) higher at 100 seconds.

The voltage waveforms of the coil with and without accounting for the temperature dependency of the B-H curve are indicated in Fig. 36. The voltage is over calculated when the temperature dependency is not taken into account. These voltage characteristics are vital when determining the inverter region to drive the induction heating device.

Therefore, analysis accounting for the temperature dependency of the B-H curve is necessary for the reason indicated above.

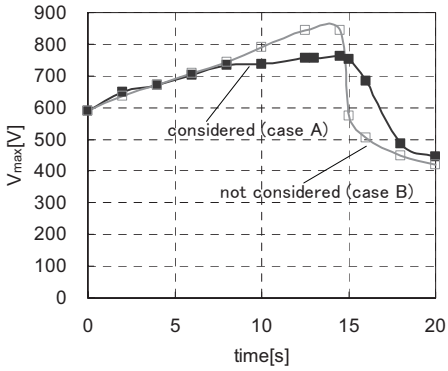

Fig. 36. Max induced voltage versus time of the coil

5. Conclusion

The knowledge gained from this paper is as follows:

(1) The accuracy of measurements was examined when measuring the material characteristics at high temperatures using a ring specimen including the effects when selecting the magnetic pathways and the expansion of the test piece caused by higher temperatures.

(2) When the magnetic field H is the same, the magnetic flux density B decreases as the temperatures rise higher than room temperature and the magnetic saturation M decreases. Furthermore, the maximum value of the relative permeability μ_s increases as the temperature rises when the magnetic flux density is small and the iron loss W is smaller than at room temperature.

(3) The iron losses are reduced by a higher relative permeability when the magnetic flux density is low

if the magnetic material is exposed to high temperatures. Therefore, the magnetic properties can be improved for devices driven at regions the magnetic flux density is relatively low after they are exposed to higher temperatures.

(4) The temperature decreases a certain amount after measuring when measuring the temperature dependency of magnetic properties of materials. The same measurement for each temperature is obtained even if the temperatures are measured by increasing the temperatures higher than the point to measure.

(5) The variations of permeability and iron loss at high temperatures differs depending on the type of magnetic material. The variations of permeability are large when exposing cold rolled steel sheet SPCC material to high temperatures to a high relative magnetic flux.

(6) Analysis results extremely close to the actual values can be obtained by running analysis that take into account the conductivity, permeability, specific heat, and thermal conductivity versus time.

(7) The skin depth increases as the resistivity increases, the permeability is reduced, the magnetic flux penetrating the billet decreases, and the heat generated in the billet is reduced by higher temperatures.

(8) The temperature is over calculated when the temperature dependency of the B-H curve is not taken into account for induction heating devices and the voltage of the coil is also over calculated.

(9) The magnetic flux primarily passes through the surface at the initial lower temperatures in the coupled magnetic field analysis accounting for the temperature distribution and the permeability distribution versus time in the axial direction of the billet, but the magnetic flux decreases as the temperature rises with time and only passes through the interior. This physical phenomena needs to be considered for the design and operation of actual billet heaters.

Reference

(1) V. Čingoski, A. Namera, K. Kaneda, and H. Yamashita: “Analysis of Magneto-Thermal Coupled Problem Involving Moving Eddy-Current Conductors– “, *IEEE Trans*. *Magn*., Vol.32, No.3, pp. 1042-1045 (1996).

(2) M. Nakaoka, A. Fukuma, H. Nakaya, D. Miyagi, M. Nakano, and N. Takahashi: “Examination of Temperature Characteristics of Magnetic Properties using a Single Sheet Tester”, IEEJ Trans. FM, vol.125, no.1, pp. 63-68 (2005).

(3) S. Kaya : ”Ferromagnetism” Iwanami Zensho (1952)

(4) M. Morishita, D. Miyagi, M. Nakano, N. Takahashi : “Examination of Magnetic Properties at Room Temperature of Non-oriented Electrical Steel having High Experience Temperature(until Curie Temperature),” The Papers of the Technical Meeting on Magnetics, IEEJ MAG-09-229, pp.29-34 (2009)

(5) M. Morishita, D. Miyagi, M. Nakano, N. Takahashi ： “Measuring Magnetic Characteristics of Magnetic Materials at High Temperatures –Method for Raising Temperatures-（磁性材料の高温での磁気特性の測定―温度上昇法の検討―),” 2009 Information Processing Society of Japan Chugoku Branch 60th Rentai，pp.520-521 (2009)

(6) N.Takahashi, M.Morishita, D.Miyagi, M.Nakano, “Examination of Magnetic Properties of Magnetic Materials at High Temperature using a Ring Specimen”, *IEEE Trans. Magn*., vol. 46, no.2, pp. 548-551 (2010)

(7) M. Morishita, D. Miyagi, M. Nonaka, N. Takashi: ”磁性材料の高温での磁気特性の比較,” 2010 Information Processing Society of Japan Chugoku Branch 61st Rentai，pp.554-555 (2010)

(8) D. Otome, Y. Yunoki, M. Nakano, D. Miyagi, N. Takahashi: ”Measurement of Magnetic Properties of Electrical Steel Sheet at Liquid Nitrogen Temperature,” The Papers of the Technical Meeting on Magnetics, IEEJ MAG-08-78，pp.7-12 (2008)

(9) D. Miyagi, D. Otome, M. Nakano, N. Takahashi: “Measurement of Magnetic Properties of Nonoriented Electrical Steel Sheet at Liquid Nitrogen Temperature Using Single Sheet Tester”, IEEE Trans. on Magn., Vol. 46, No. 2, pp.314-317 (2010)

(10) N. Takahashi: “Fundemental Magnetic Field Analysis Technology Using the Finite Element Method (三次元有限要素法-磁界解析技術の基礎)” IEEJ (2006)

(11) N. Takahashi, D. Miyagi, N. Uchida, K. Kawanaka: “Electromagnetic-thermal Coupled Analysis of Billet Heater for Heating before Forging,” Mitsui Zosen Technical Review, No.196, pp.31-37 (2009)

(12) H. Kurose, D. Miyagi, N. Takahashi: “3D Eddy Current Analysis of Induction Heating Apparatus Considering Heat Emission, Heat Conductivity, and Temperature Dependence of Magnetic

Characteristics," The Papers of Joint Technical Meeting on Magnetics, Static Apparatus, and Rotating Machinery, IEEJ MAG-08-34, SA-08-22, RM-08-22, pp.51-56 (2008)
(13) W. H. Giedt: "Principles of Engineering Heat Transfer," Maruzen (1960)
(14) E. Kuroda: "3D Heat Transfer Analysis Program Using Visual Basic (Visual Basic による 3 次元熱伝導解析プログラム),"CQ Publishing (2003)
(15) The Japan Society of Mechanical Engineers: "Heat Transfer," Maruzen (1987)
(16) H. Kurose, D. Miyagi, N. Takahashi, N. Uchida: "Coupled Electromagnetic Field and Thermal Analysis of Induction Heating Apparatus Accounting for the Temperature Dependency of Magnetic Characteristics (磁気特性の温度依存性まで考慮した誘導加熱装置の電磁場- 温度場連成解析)," Annual Meeting of the IEEJ, 5-192, pp.284-285 (2008)
(17) H.Kurose, D. Miyagi, N. Takahashi, N. Uchida, and K. Kawanaka : "3-D Eddy Current Analysis of Induction Heating Apparatus Considering Heat Emission, Heat Conduction, and Temperature Dependence of Magnetic Characteristics", *IEEE Trans. Magn.,* vol. 45, no.3, pp. 1847-1850 (2009).
(18) H. Kagimoto, N. Takahashi, D. Miyagi, N. Uchida, K. Kawanaka: "Characteristic Analysis of an Induction Heating Apparatus Accounting for the Temperature Dependency of Magnetic Characteristics –Effects of the Temperature Dependency on Magnetic Characteristics- (磁気特性の温度依存性を考慮した誘導加熱装置の特性解析 -磁気特性の温度依存性の影響-)," 2010 Information Processing Society of Japan Chugoku Branch Rentai, pp.522-523 (2009)
(19) H. Kagimoto, D. Miyagi, N. Takahashi, N. Uchida, K. Kawanaka: "Effect of Temperature Dependence of Magnetic Properties on Heating Characteristics of Induction Heater", IEEE Trans. on Magn., Vol.46, No. 8, pp.3018-3021 (2010)
(20) M. Morishita, N.Takahashi, D.Miyagi, M.Nakano: " Examination of Magnetic Properties of Several Magnetic Materials at High Temperature", Proc. 11th Int. Workshop on 1&2 Dimensional Magnetic Measurement and Testing (2010)
(21) S. Chikazumi: "Principles of Ferromagnetic Bodies (強磁性体の物理)," Shokabo Publishing (1984)